TWENTYFIFTH EUROPEAN ROTORCRAFT FORUM

Paper no. C2

# Normal Vortex Interaction with a Loaded Symmetrical Blade

BY

C.J. DOOLAN, F.N. COTON & R.A.McD. GALBRAITH
Department of Aerospace Engineering
University of Glasgow
Scotland, UK

SEPTEMBER 14-16, 1999
ROME
ITALY

ASSOCIAZIONE INDUSTRIE PER L'AEROSPAZIO, I SISTEMI E LA DIFESA
ASSOCIAZIONE ITALIANA DI AERONAUTICA ED ASTRONAUTICA

# Normal Vortex Interaction with a Loaded Symmetrical Blade

C.J. Doolan, F.N. Coton and R.A.McD. Galbraith
Department of Aerospace Engineering
University of Glasgow
Glasgow, Scotland, UK

## 1. Abstract

The results of an experimental programme into the aerodynamic effects of a normal vortex interaction with a blade set at various degrees of incidence are presented. Surface pressure data revealed that the aerodynamic response was dominated by the effects of the vortex core axial flow. When the blade was aerodynamically loaded, the surface pressure measurements were perturbed from the results obtained at zero incidence. This perturbation was dependent on the sign and magnitude of the blade incidence and was always mirrored by a corresponding change on the opposite surface which maintained the relative peak magnitude of normal force. The normal force quickly increased when the vortex impacted with the leading edge and the quarter chord pitching moment also showed a very fast nose up moment, followed by a rapid nose down moment.

## 2. Nomenclature

| | |
|---|---|
| $C_n$ | normal force coefficient |
| $C_m$ | quarter chord pitching moment coefficient |
| $C_p$ | pressure coefficient, $\frac{p_u - p_\infty}{\frac{1}{2}\rho V_\infty^2}$ |
| $c$ | interacting blade chord, m |
| $p$ | pressure, Pa |
| $R$ | rotor radius, m |
| $r_c$ | vortex core radius |
| $t$ | time, s |
| $V$ | velocity, $ms^{-1}$ |
| $x$ | distance, m |
| $\alpha$ | angle of incidence, deg |
| $\Gamma$ | circulation, $m^2s^{-1}$ |
| $\Omega$ | rotor angular velocity, $rads^{-1}$ |
| $\rho$ | freestream density, $kgm^{-3}$ |
| $\nu$ | kinematic viscosity, $m^2s^{-1}$ |

Subscripts

| | |
|---|---|
| $s$ | time averaged measurement |
| $u$ | measurement made during interaction |
| $\infty$ | freestream conditions |

## 3. Introduction

The interactional aerodynamics of rotorcraft play a significant role in the generation of unwanted noise and vibration. A well known example of this this occurs between the main rotor and its own wake structure which has been intensively studied in the past. Less understood is the case of the tail rotor interacting with the main rotor wake which can produce radiated noise, structural vibration and, in some cases, a degradation in lateral control effectiveness. In such an interaction, the main rotor trailing vortex collides with a tail rotor blade orthogonally and is eventually 'cut' or severed into two parts (see Fig. 1).

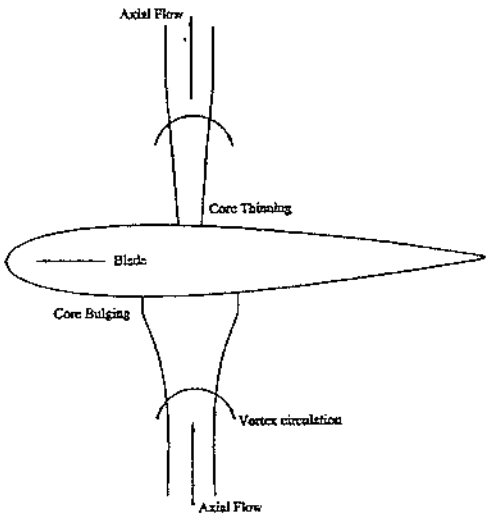


Figure 1: Illustration of vortex dynamics during vortex cutting.

Previous work on this type of vortex interaction has involved acoustic studies[1–3] and practical flight trials.[4–6] Fluid dynamic studies have concentrated on the interaction of a rotor tip vortex and a large cylinder, representative of the helicopter fuselage.[7–10] Flow visualisation experiments have also been performed by Marshall and Krishnamoorthy[11,12] in support of a computational model of the orthogonal vortex interaction. Qualitatively, these studies have shown that once the vortex has been cut or 'chopped' by a solid surface, the vortex core size increases or 'bulges' on one side of the surface and decreases or 'thins' on the other. The behaviour of the vortex core is shown to be controlled by the direction of vortex core axial flow. Flow visualisation and surface pressure measurements of the interaction of a wing with a propeller wake[13] also show this change in vortex core size.

Recently, measurements of the interaction with a blade at zero incidence were described by Doolan *et al.*[14] It was found that a pressure pulse occurred on the side of the blade where the axial flow was expected to travel towards the surface and a suction peak on the side where the axial flow was away from the surface. Here this work is extended to show the interaction with a loaded blade. An instrumented blade, set at various degrees of incidence, was placed in the path of a convecting rotor tip vortex to measure the normal blade vortex interaction. Observations of the transient pressure data revealed the aerodynamic response of the blade to a vortex cut. Surface pressure measurements were also integrated to yield force and pitching moment data.

## 4. Experiment

The experiments were conducted in the Glasgow University 1.15 m x 0.85 m low speed wind tunnel. This is a closed return facility with a working section length of 1.8 m and is capable of speeds up to 33 $ms^{-1}$. During testing, the free-stream velocity and temperature were monitored continuously using a pitot-static tube and thermocouple device located in the working section.

The design of the vortex generator has been previously detailed by Copland[15] but will, for convenience, be summarised here. The vortex generator is essentially a rotor of radius 0.75 m that has a single rectangular planform blade of chord 0.1 m with a NACA 0015 cross section. During rotation, the blade pitch is varied using a spring loaded pitch link running on a cylindrical cam configured such that the blade pitch varies in four equivalent (90°) phases of azimuth. The first phase sets the blade at zero incidence while the blade is pointing into the settling chamber (45° azimuthal travel on either side of the wind tunnel centre line). In the next two phases of motion, the blade is pitched from zero to 10°, before traversing the working

Table 1: Maximum blade tip non-dimensional operating parameters.

| | |
|---|---|
| Tip Mach Number | 0.18 |
| Tip Reynolds Number | $3.95 \times 10^5$ |
| Tip Vortex Strength $(\frac{\Gamma}{cR\Omega})$ | 0.47 |
| Tip Vortex Reynolds Number $(\frac{\Gamma}{\nu})$ | $1.3 \times 10^5$ |

section at a constant $10^o$ incidence. In the final $90^o$ phase, the spring loaded pitch link forces the blade to overcome its aerodynamic and inertial loads and follow the cam as it returns to zero degrees.

The rotor assembly is mounted on a vertical rotating shaft which is supported by bearings which are installed in an external framework above and below the wind tunnel contraction. Also located on this framework is a DC electric motor which is used to drive the rig. During operation the rotational speed is monitored by an optical sensor located on the main shaft.

The vortex generator produces a curved, three-dimensional vortex which convects through the wind tunnel working section. A NACA 0015 blade of chord 152.4 mm and overall span 944 mm was placed in the path of the convecting vortex in order to study the interaction of the vortex with the blade. The experimental setup allowed a variation of the geometric incidence of the blade. Measurements were obtained within a blade incidence range of $\pm 10^o$ using $2^o$ increments. When set at $0^o$, the leading edge of the blade was 2000 mm or 13.12 blade chord lengths downstream of the rotor centre line. The blade was instrumented at 78.5% span with a chordal array of 30 miniature Kulite pressure transducers mounted around the surface of the blade.

For the current test programme the freestream velocity was fixed at 20 $ms^{-1}$ and the rotational speed of the vortex generator was 500 RPM. These settings had been previously identified by Doolan *et al.*[16] to provide a clear, well defined tip vortex structure in the working section. Based on these conditions, the nominal interacting blade Reynold's number was $2 \times 10^5$. Operating parameters for the transverse vortex generator are displayed in Table 1 and were determined using a numerical procedure outlined in Doolan *et al.*[14]

As shown schematically in Fig. 2, the blade was mounted from the roof of the working section and extended to the tunnel floor. To facilitate the change in incidence of the blade, a specially designed support was located on the tunnel floor. Also, the blade was placed 225 mm from the tunnel centreline (Fig. 3) at $x_b/c = \pm 1.48$ in order to avoid the turbulent wake of the vortex generator support shaft. Previous velocity measurements have shown that the vortex is obscured by this wake.[16]

The height of the stationary blade was set such that the chordwise transducers were positioned in the path of the vortex core. This position was determined using the results of a hot wire probe survey as described Doolan *et al.*[14]

Pressure data were recorded using a BE256 data logger in a single 32000 sample block at 20 kHz sampling rate. This sample rate and size allowed approximately 13 rotor revolutions of data capture. Five blocks of data were obtained at each blade incidence.

The BE256 data logger and software employs an automatic gain adjustment feature which allows measurements to be taken at the maximum accuracy possible for the system. On the basis of previous experience with the Kulite miniature transducers[17] and taking account of discretisation and calibration factor errors, the uncertainty in the measured pressure coefficient was estimated at 0.5%. Using a similar technique to Baines *et al.*,[18] the maximum uncertainty in the force and pitching moment coefficients was estimated to be 2.1%.

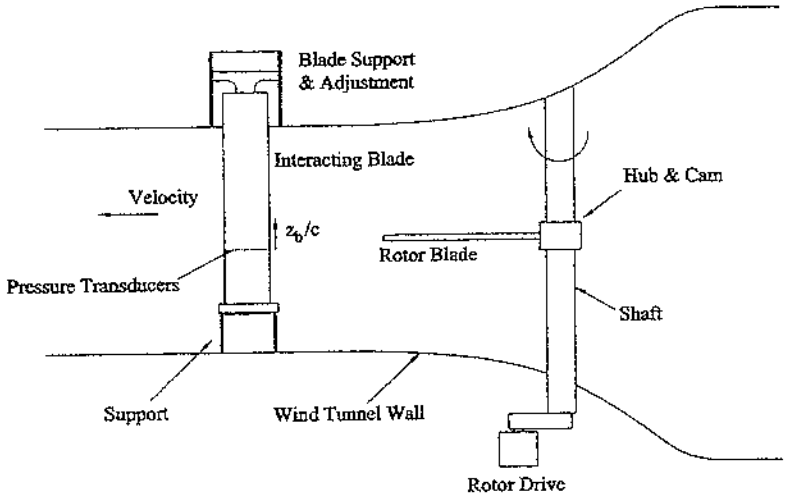


Figure 2: Schematic showing vortex generator and interacting blade.

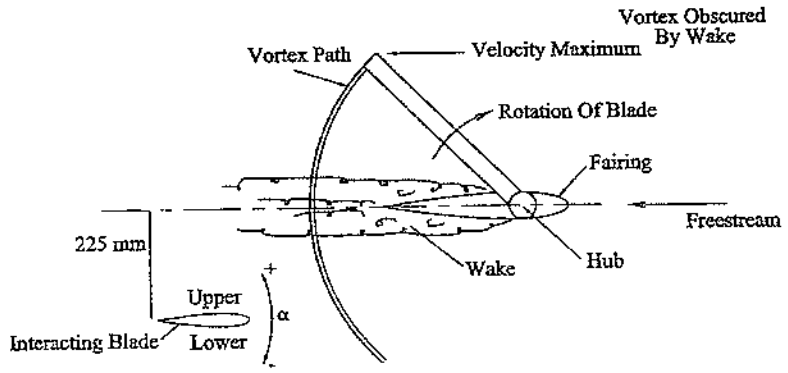


Figure 3: Plan view of wind tunnel showing interacting blade position.

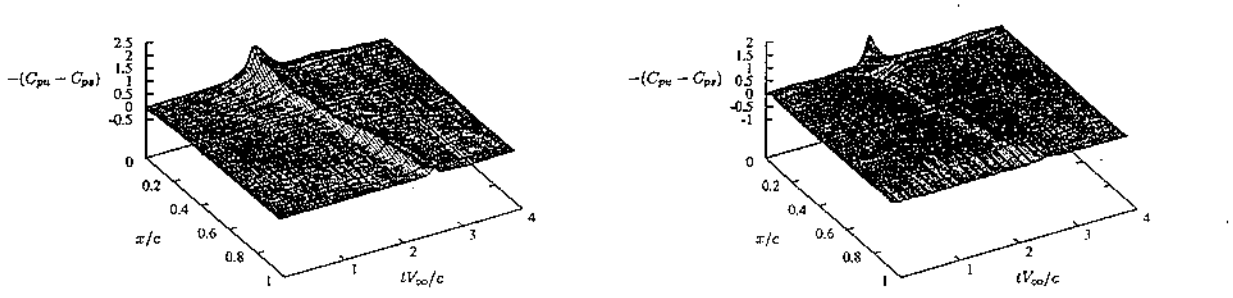


(a) **Upper surface.** (b) **Lower surface.**

Figure 4: Unsteady pressure measurements on blade surface, $\alpha = 0^o$.

The largest source of error in the measurements was vortex position. Once produced by the rotor rig, the vortex is free to convect through the wind tunnel. Each successive vortex follows a slightly different path due to variations in local conditions about the rotor blade and freestream turbulence levels. The wandering amplitude of the vortices has been estimated at 19% of the interacting blade chord using hot wire measurements of the vortex dimensions and a numerical procedure.[16] The wandering imparts uncertainty regarding the location of the vortex relative to the transducer array. Accordingly, 65 interactions were recorded at each test position and from these results were extracted representative data sets at the quoted transducer locations.

## 5. Results

The upper and lower surfaces of the blade are defined in Fig. 3 as are the directions of positive and negative blade incidence. A previously performed hot wire survey of the vortex generator wake[16] found that the wake was asymmetric about the tunnel centre. The wake geometry determines the approach angle of the vortex with the interacting blade and for the present experiments, it can be shown that the vortex approaches the blade at approximately $90^o$ when it is set at zero incidence.

Hot wire measurements[14] of the vortex structure were used to determine the vortex core size ($r_c/c$=0.065) and the blade impact parameter ($2\pi r_c V_\infty/\Gamma = 2.91$). The blade impact parameter has been identified by Marshall and Krisnamoorthy[11] as a quantity which indicates the severity of the physical response to the vortex cut. The value obtained here implies that a weak interaction occurs during the experiments with no boundary layer separation. It has been shown by Krisnamoorthy and Marshall[12] that the weak vortex interaction is the dominant tail rotor interaction mechanism for a helicopter in forward flight with an advance ratio greater than approximately 0.1.

Figure 4 illustrates the temporal variation of the pressure data recorded as the vortex is cut by a blade set at zero incidence. In each plot, the time averaged component of the pressure signal has been removed in order to increase the clarity of the results. The time averaged component ($C_{ps}$) was determined by averaging the 32000 pressure samples obtained during each test. Hence, $-(C_{pu} - C_{ps})$ is plotted on the vertical axis with the chord position of the transducers ($x/c$) on one axis and non-dimensional time ($tV_\infty/c$) on the axis in the foreground. To further increase the clarity of the plots only every fifth data sample is presented.

The upper surface interaction data in Fig. 4(a) show a strong suction peak at the leading edge when the vortex first encounters the blade. As the vortex passes over the surface, this

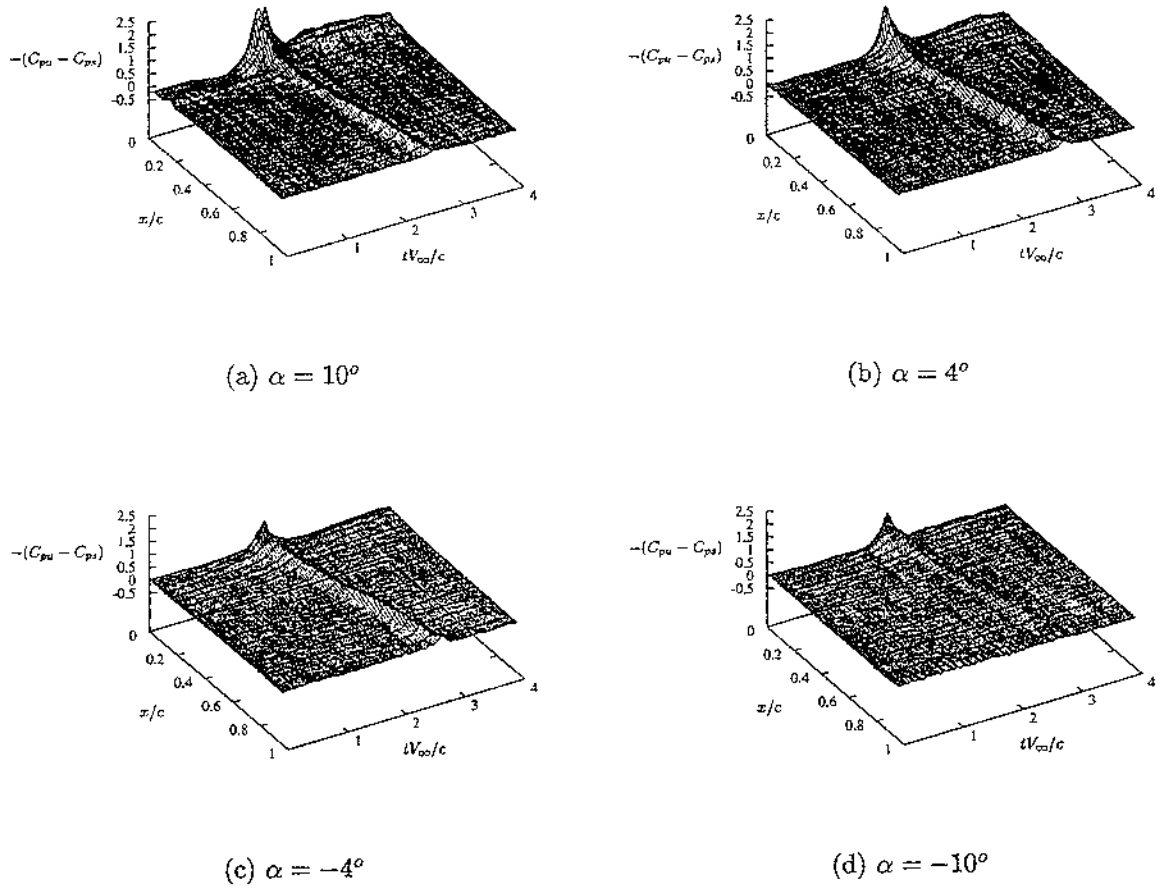


(a) $\alpha = 10^o$ (b) $\alpha = 4^o$

(c) $\alpha = -4^o$ (d) $\alpha = -10^o$

Figure 5: Unsteady pressure measurements on upper surface of loaded blade.

suction peak diminishes but remains prominent over the rest of the chord.

For the lower surface (Fig. 4(b)), an increase in pressure occurs just downstream of the leading edge but is rapidly reduced in magnitude as the vortex travels over the blade surface. At approximately the quarter chord point, the pressure ridge transforms into a slight suction ridge which convects over the chord. In the lower surface plots, the leading edge pressure record is repeated for completeness.

Results of the vortex interaction with a loaded blade at a selection of incidence settings are shown in Figs. 5 and 6. On the upper surface, the suction peak at the leading edge intensifies with increasing positive incidence (Fig. 5(a) and (b)). The suction ridge over the remaining blade surface also increases in strength at $\alpha = 4^o$, but diminishes at $\alpha = 10^o$. When the incidence is changed to a negative value (Fig. 5(c) and (d)), the leading edge suction ridge reduces in magnitude. The suction ridge over the rest of the blade also becomes weaker with increased negative incidence.

On the lower surface, the change in incidence has a similar effect on the observed pressure pulse. As the incidence is increased in the positive sense (Fig. 6(a) and (b)) the pressure pulse is reduced. When the incidence becomes negative (Fig. 6(c) and (d)), the pressure pulse at the leading edge increases in magnitude. The mild suction ridge which appears after the initial pressure pulse tends to diminish with increasing incidence magnitude.

The surface pressure results obtained are interesting and illustrate the complexity of the vortex interaction. Common to all records is the presence of a suction peak on the upper surface

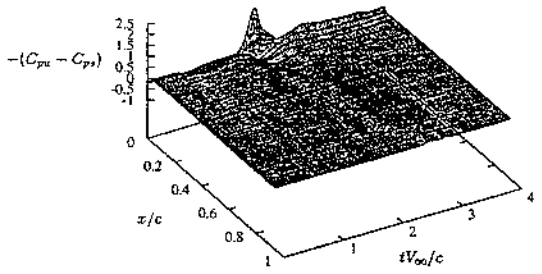


(a) $\alpha = 10^o$

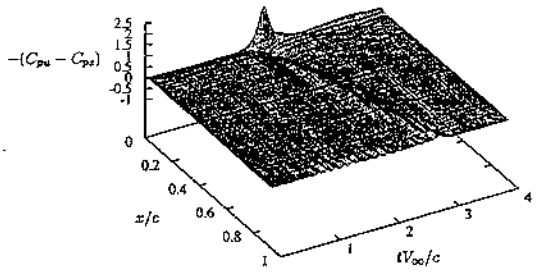


(b) $\alpha = 4^o$

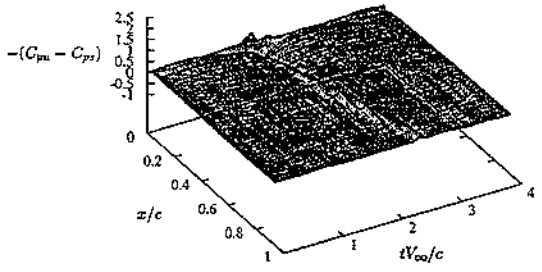


(c) $\alpha = -4^o$

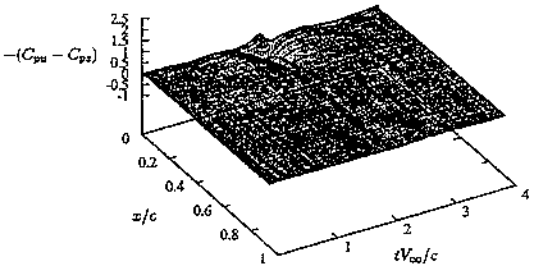


(d) $\alpha = -10^o$

Figure 6: Unsteady pressure measurements on lower surface of loaded blade.

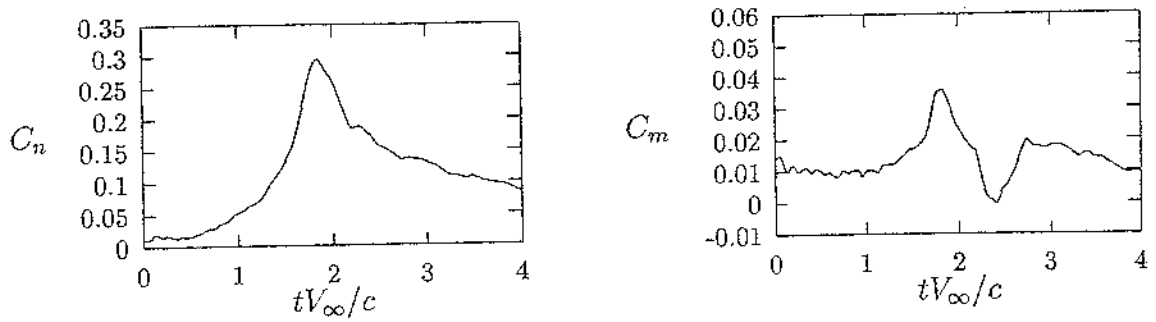


(a) (b)

Figure 7: (a) Normal force and (b) quarter chord pitching moment data, $\alpha = 0^o$.

and a pressure peak on the lower surface in the vicinity of the leading edge. This aerodynamic response can be explained in terms of the core axial flow.[14] For the current configuration, the vortex axial flow is expected to travel towards the lower surface and away from the upper surface hence initiating the pressure and suction peaks observed.

When placed at some incidence, the differences in the observed pressure records are more difficult to explain. The amplification and attenuation of leading edge suction and pressure peaks may be due to the local change in incidence caused by the vortex core axial component. Also, the induced tangential velocity field of the vortex may interact with the spanwise flow on the loaded blade surfaces to produce additional pressure components. At this stage, there is no comprehensive theory which can explain the observed results and more investigation is necessary.

By integrating the pressure data, transient normal force and quarter chord pitching moment coefficients of the vortex interaction can be studied. Figure 7 shows the force and moment coefficient data against non-dimensionalised time for the unloaded blade. A sharp rise in normal force occurs as the vortex collides with and is cut by the blade. The quarter chord pitching moment data also shows a sharp nose-up moment as the vortex arrives at the leading edge. The value of the pitching moment then falls as the vortex passes over the quarter chord point, before re-establishing itself at the pre-interaction level as the vortex passes beyond the trailing edge. Although, the suction peak is only small over the trailing edge, the moment arm is long, hence the significant effect on the pitching moment.

The effect of changing incidence on normal force produced by the interaction is shown in Fig. 8. The sharp rise in normal force is maintained in all cases and the change in magnitude is also approximately the same. In each figure, the relative range of the vertical axes remains the same, however each is offset by a different amount due to the static loading on the blade at each incidence setting. Variations in the interaction response at the same incidence setting are thought to be due to vortex wandering. The loading history is similar for most angles of incidence, with a region of unsteadiness following the main interaction which is associated with the turbulent vortex sheet which follows the convecting tip vortex through the working section.

Figure 9 displays the mean rise in normal force coefficient, $\Delta C_n$, obtained for all values of incidence used in the test programme. The value $\Delta C_n$ is defined as the difference between the peak normal force coefficient value during an interaction and the time averaged value for the entire test which effectively removes the static offset for each blade incidence setting. Each data point in Fig. 9 represents the average of sixty peak normal force measurements taken during

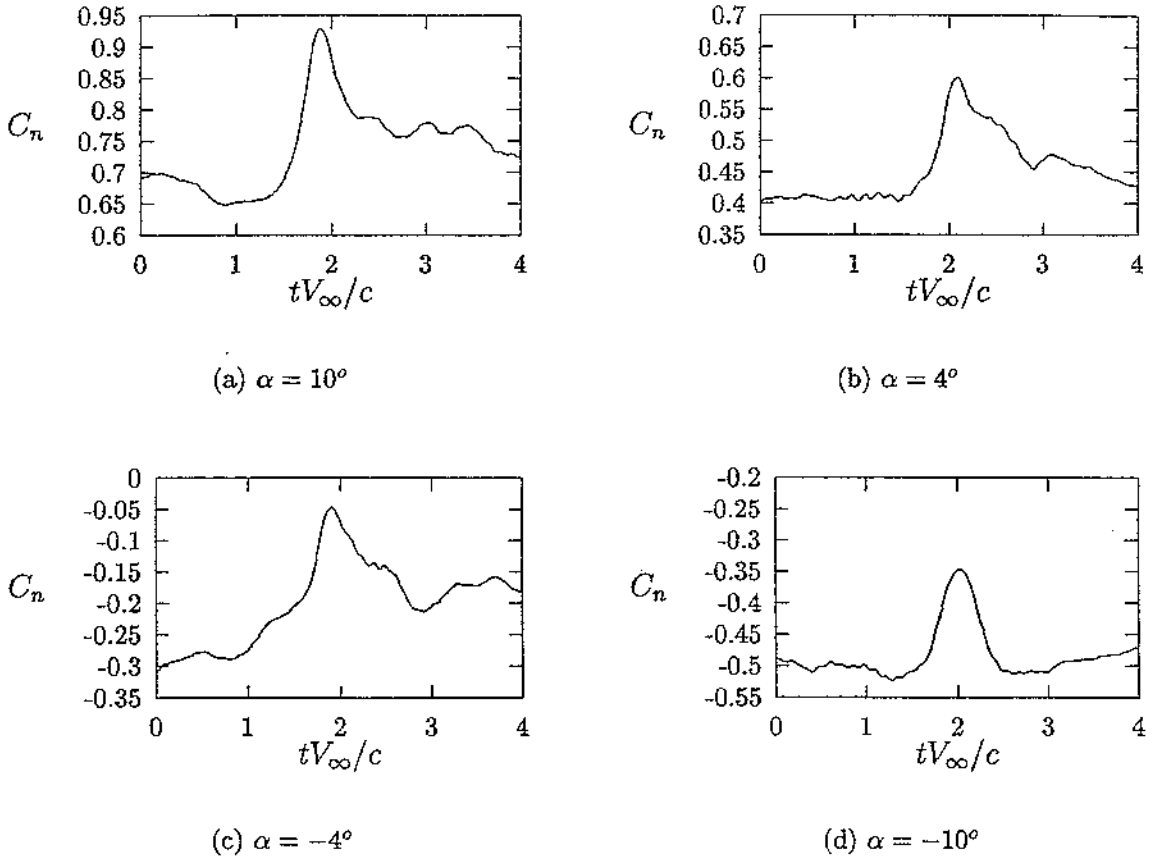


(a) $\alpha = 10^o$

(b) $\alpha = 4^o$

(c) $\alpha = -4^o$

(d) $\alpha = -10^o$

Figure 8: Normal force measurements on loaded blade.

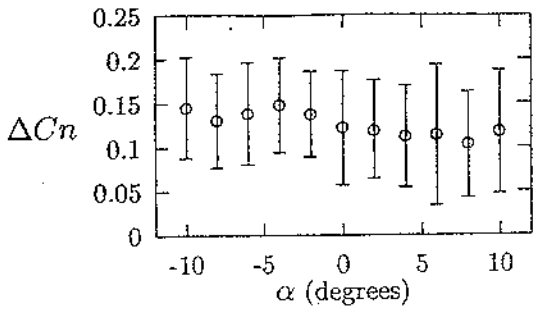


Figure 9: Change in normal force experienced by blade during interaction.

the vortex interaction. The error bars indicate one standard deviation of the sample and give an estimate of the effect of vortex wandering on the test results. Although the results show a minor change over the test range, $\Delta C_n$ can be regarded as remaining approximately the same as the incidence is changed.

Quarter chord pitching moment data for the case of a loaded blade is shown Fig. 10. The results show that for most incidence settings, the pitching moment history is approximately similar to the zero incidence case with a sharp increase as the vortex approaches and a sudden decrease as the vortex core moves over the quarter chord point. However at $\alpha = -10^o$ the pitching moment is much reduced and perhaps represents the limits of a region of the interaction at small incidence where the aerodynamic response is a perturbation of the results obtained at $\alpha = 0^o$. It is recommended that further studies be performed at higher incidence to determine if this is the case.

## 6. Conclusions

An experiment was performed where a convecting rotor tip vortex collided with an instrumented, stationary NACA 0015 profile blade which was set at incidences between $\alpha = \pm 10^o$. Results at zero incidence indicate that suction peaks and pressure pulses at the leading edge can be explained in terms of the core axial flow component impacting on the surface. It was found that a change in incidence perturbs the interaction response from the $\alpha = 0^o$ case in different ways depending on the sense of the blade incidence.

Interestingly, the change in pressure response on the upper surface was mirrored by a similar effect on the lower surface which kept the relative rise in normal force approximately constant for the incidence range used here. It is suggested that this effect may be caused either by a local change in effective incidence due to the approaching core axial flow or by an interaction of the vortex tangential velocity component with the spanwise flow on the loaded blade. The exact detail is at this stage unclear and further experimentation and analysis is required to explain this phenomenon. As part of the tail rotor vortex interaction research project at Glasgow University, it is planned to implement non-intrusive flow measurement techniques to visualise and quantify the interaction vortex dynamics and to install additional spanwise instrumentation to resolve any spanwise convection of the vortex over the blade surface. It is hoped through application of these techniques a better understanding of the normal vortex interaction will be attained.

Acknowledgements: This work was funded by the Engineering and Physical Sciences Reseach Council, the Defence Evaluation and Research Agency, Farnborough and GKN-Westland Helicopters Ltd under grant number GR/L 58231. The authors would also like to thank Dr. C. Copland for the design of the vortex generator rig and Mr. R. Gilmour and Mr. D. Perrins for their

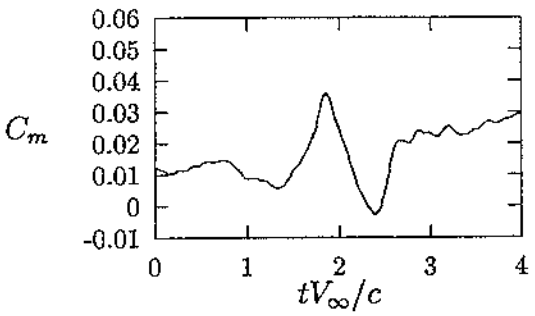


(a) $\alpha = 10^o$

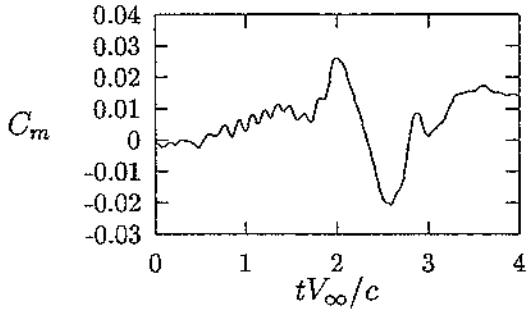


(b) $\alpha = 4^o$

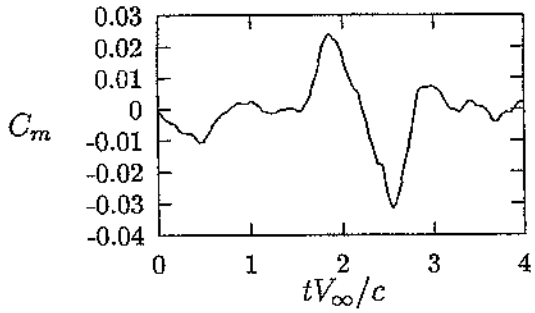


(c) $\alpha = -4^o$

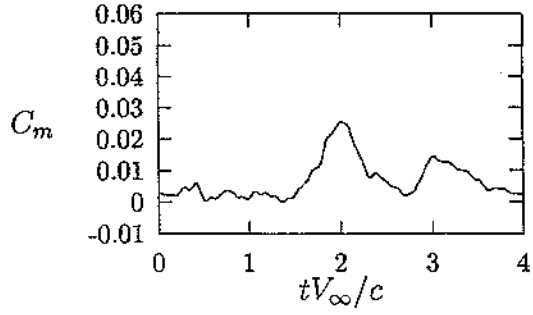


(d) $\alpha = -10^o$

Figure 10: Quarter chord pitching moment measurements on loaded blade.

technical assistance.

## 7. References


1. Samokhin, V.F. Impulsive noise of the helicopter tail rotor, 21st European Helicopter Forum, St-Petersberg, Russia, Aug-Sept, 1995.
2. Schultz, K.J. and Splettstoesser, W.R. Helicopter main rotor/tail rotor noise radiation characteristics from scaled model rotor experiments in the DNW, 49th Annual Forum of the American Helicopter Society, St-Louis, USA, May 1993.
3. Howe, M.S. On unsteady surface forces and sound produced by the normal chopping of a rectilinear vortex, *J Fluid Mech*, 1989, 206, pp 131-153.
4. Jacobs E.W., Mancini, J., Visintainer, J.A. and Jackson, T.A. Acoustic flight test results for the Sikorsky S-76 quiet tail rotor at reduced tip speed, 53rd Annual Forum of the American helicopter Society, Virginia Beach, USA, April-May 1997.
5. Leverton, J.W. and Pike, T.C. The importance of tail rotor interaction as an acoustic source, 49th Annual Forum of the American Helicopter Society, St-Louis, USA, May 1993.
6. Ellin, A.D.S. An in flight Study of Lynx AH MK5 main rotor/tail rotor interactions, 19th European Helicopter Forum, Cernobbio, Italy, September, 1993.
7. Liou, S.G., Komerath, N.M. and McMahon, H.M. Measurement of the interaction between a rotor tip vortex and a cylinder, *AIAA J*, 1990, 28, (6), pp 975-981.
8. Affes, H., Conlisk, J.M., Kim, J.M. and Komerath, N.M. Model for rotor tip vortex-airframe interaction part 2: Comparison with experiment, *AIAA J*, 1993, 31, (12), pp 2274-2282.
9. Affes, H., Xiao, Z., Conlisk, A.T., Kim, J.M and Komerath, N.M. Model for rotor tip vortex-airframe interaction part 3: Viscous flow on airframe, *AIAA J*, 1998, 36, (3), pp 409-415.
10. Bi, N., Leishman, J.G. and Crouse, G.L. Investigation of rotor tip vortex interactions with a body, *J Aircraft*, 1993, 30, (6), pp 879-888.
11. Marshall, J.S. and Krishnamoorthy, S. On the instantaneous cutting of a columnar vortex with non-zero axial flow, *J Fluid Mech*, 1997, 351, pp 41-74.
12. Krishnamoorthy, S. and Marshall, J.S. Three-dimensional blade vortex interactions in the strong vortex regime, *Physics of Fluids*, 1998, 10, (11), pp 2828-2845.
13. Johnston, R.T. and Sullivan, J.P. Unsteady wing surface pressures in the wake of a propeller, AIAA Paper 92-0277, AIAA 30th Aerospace Sciences Meeting, Reno, USA, January 1992.
14. Doolan, C.J., Coton, F.N. and Galbraith, R.A.McD. Three-dimensional vortex interactions with a stationary blade. Submitted to*Aeronaut J*, 1999.
15. Copland, C.M. Methods of generating vortices in wind tunnels, PhD thesis Department of Aerospace Engineering, University of Glasgow, 1997.
16. Doolan, C.J., Coton, F.N. and Galbraith, R.A.McD. Measurement of three-dimensional vortices using a hot wire anemometer, AIAA Paper 99-3810, AIAA 30th Fluid Dynamics Conference, June/July 1999.
17. Masson, C.A., Green, R.B., Galbraith, R.A.McD. and Coton, F.N. Experimental investigation of a loaded rotor blade's interaction with a single vortex, *Aeronaut J*, 1998, 102, (1018), pp 451-457.
18. Baines, N.C., Mee, D.J. and Oldfield, M.L.G. Uncertainty analysis in turbomachine and cascade testing, *Int J Eng Fluid Mech*, 1991, 4, (4), pp 375-401.